Wave-Generated Disturbance Downstream of a Nozzle Array

T. S. Vaidyanathan* and David A. Russell†
University of Washington, Seattle, Washington

Waves resulting from the expansion process are an important source of nonhomogeneity in the supersonic flow downstream of nozzle arrays. Flows from radial nozzles are analyzed by a small-perturbation procedure that yields the first solutions for the near field in the two-dimensional case and for the entire field in three dimensions. Good agreement is found with method-of-characteristics calculations and with earlier interferometric measurements of integrated density disturbance. The complete solutions bring out the dependence of flow quality on nozzle dimension, Mach number, expansion angle, and ratio of specific heats. Application to laser cavity flow is discussed.

Nomenclature

C_1,C_2,C_3,C_6 = constants of integration [Eqs. (18c) and (33)]
C_4,C_5 = n-dependent constants [Eq. (20b)]
C_v = specific heat at constant volume
D_1,D_2,D_3 = constants [Eqs. (11c), (17), and (33)]
F,G,H = functions [Eq. (31) and Fig. 4]
j = index, = 0 for 2-D, 1 for 3-D
ℓ = distance along optical path
M = Mach number
n = cell number (Fig. 2)
p = static pressure nondimensionalized by p at origin
S = shock shape function [Eq. (12)]
s = entropy/mass
u,v,w = Cartesian velocity components nondimensionalized by u at origin
x,y,z = Cartesian coordinates (Figs. 2 and 3) nondimensionalized by nozzle half-height
$\tilde{x}$ = $x-(n-1)\beta$, axial distance from cell center
α = angle between shock and x axis
$\alpha_1,\alpha_2,\alpha_3$ = angle coefficient [Eqs. (24) and (34)]
β = $\sqrt{M_e^2-1}$
γ = ratio of specific heats
δ = 0 for n odd, 1 for n even
ϵ = source flow half-angle (Fig. 2)
ρ = density nondimensionalized by ρ at origin
ϕ = optical axis angle at nozzle exit (Fig. 9)
χ = $\beta^{-1}x-(n-1)$ for n even

Subscripts

d = downstream of shock
e = value at origin ($x,y,z=0$)
max = maximum local value in a cell
s = on the shock
u = upstream of shock
0 = perturbed coordinate [Eq. (5)]
$1,2,3,\ldots$ = order or perturbation term

I. Introduction

NOZZLE arrays are commonly used in high-power continuous-wave gas lasers, and they have application to other gas processes requiring small-scale mixing or rapid expansion to supersonic flow. In such arrays, the flow exiting individual nozzles is typically divergent and forced by the presence of neighboring streams to turn through shock waves originating near the nozzle trailing edges. These shocks reflect between planes of symmetry downstream and decay slowly through subsequent nonlinear interaction. The pattern of waves is shown for the two-dimensional (2-D) case in Fig. 1. Nozzle arrays must also produce wake-like disturbances originating with the nozzle boundary layers. While the latter are clearly seen in schlieren photographs of 2-D flow,[1] studies by Russell et al.[2] have indicated that the waves can be the dominant flow feature. The analytical prediction of the decaying wave system and the resulting flow is the subject of the present paper.

Linearization of the nonlinear partial differential equations of inviscid supersonic flow leads to a wave system which remains unattenuated for all distances downstream. Hence, any attempt to calculate decaying disturbances must be fundamentally nonlinear. Some plate and axisymmetric wave decay problems have been solved using approximate methods,[3-5] with particular attention to the attenuation of a single shock by interaction with downstream characteristics. Whitham,[6] for example, formulated the rule that the effects of nonlinearity can be accounted for by applying the results of linear theory along characteristics whose locations are correctly determined to first-order accuracy. Coupling Whitham's rule with a further assumption based on physical reasoning, Simons[7] obtained the far-field decay from a plane nozzle array. The solution is ingenious and applicable to a variety of exit flows; however, it is restricted due to the absence of a near-field solution, and the effect of 3-D geometry is not considered. The present study is concerned with solutions of the whole flowfield downstream of source-like nozzle arrays for 2-D and for a representative 3-D configuration.

The extent to which a line source in 2-D and a point source in 3-D can represent the actual exit flow from an array nozzle depends on the wall contour. Method-of-characteristics calculations for a straight-sonic-line conical nozzle with a half-angle of 30 deg, ratio of specific heats of 1.4, and ideal exit Mach number of 3.0, predict a maximum deviation from conical source flow values of 20% in the flow angle and 10% in the Mach number on the exit arc. Two-dimensional nozzles would have less deviation, as would those with less extreme angle or with sonic curved lines. For truncated contoured nozzles the effective expansion angle will be quite small, but representation as a source flow should provide a reasonable and consistent description of the exit flow.

Section II develops the mathematical problem, followed by Secs. III and IV on the plane nozzle array and 3-D wave decay, respectively. A discussion and application section precedes the conclusions.

Received Dec. 6, 1983; revision received July 13, 1984.

*Graduate Student, Aerospace and Energetics Research Program; presently Research Scientist, Analytical Methods, Redmond, Wash. Member AIAA.

†Professor and Chairman, Department of Aeronautics and Astronautics. Associate Fellow AIAA.

II. The Mathematical Problem

Figure 2 illustrates the problem to be studies. Due to symmetry, only the source-flow of half-angle ϵ need be considered. The coordinate system is set up with x as the downstream distance measured from the nozzle exit plane.

Conservation of mass and momentum for a steady inviscid flow results in

$$\frac{\partial \rho u}{\partial x}+\frac{\partial \rho v}{\partial y}+j\frac{\partial \rho w}{\partial z}=0 \tag{1}$$

and

$$u\frac{\partial u}{\partial x}+v\frac{\partial u}{\partial y}+jw\frac{\partial u}{\partial z}=-(\gamma M_e^2)^{-1}\rho^{-1}\frac{\partial p}{\partial x}$$

$$u\frac{\partial v}{\partial x}+v\frac{\partial v}{\partial y}+jw\frac{\partial v}{\partial z}=-(\gamma M_e^2)^{-1}\rho^{-1}\frac{\partial p}{\partial y}$$

$$j\left(u\frac{\partial w}{\partial x}+v\frac{\partial w}{\partial y}+w\frac{\partial w}{\partial z}\right)=-(\gamma M_e^2)^{-1}\rho^{-1}\frac{\partial p}{\partial z} \tag{2}$$

connecting the nondimensional Cartesian velocity components (u,v,w) and the nondimensional density ρ, and pressure p. The dependent variables are nondimensionalized by u, ρ, and p at the origin, the independent variables by the half-height of the nozzle exit. M_e is the nozzle exit Mach number at the origin of the coordinates, while the index j is zero for 2-D flow and unity for 3-D. γ is the ratio of specific heats.

The dimensionless entropic equation of state for a calorically and thermally perfect gas may be written as

$$p=\rho^{\gamma}e^{s/C_v} \tag{3}$$

where s is the entropy per unit mass and C_v the specific heat at constant volume. This relation may be used to replace the derivatives of p in Eqs. (2) with derivatives of ρ and s.

For small ϵ, the flow variables downstream of the nozzle may be expressed as perturbation expansions in ϵ. Then,

$$u=1+\epsilon u_1(x,y,jz)+\epsilon^2 u_2(x,y,jz)+\dots$$

$$v=\epsilon v_1(x,y,jz)+\epsilon^2 v_2(x,y,jz)+\dots$$

$$w=j\epsilon w_1(x,y,jz)+j\epsilon^2 w_2(x,y,jz)+\dots$$

$$\rho=1+\epsilon\rho_1(x,y,jz)+\epsilon^2\rho_2(x,y,jz)+\dots$$

$$p=1+\epsilon p_1(x,y,jz)+\epsilon^2 p_2(x,y,jz)+\dots$$

$$s=\epsilon s_1(x,y,jz)+\epsilon^2 s_2(x,y,jz)+\epsilon^3 s_3(x,y,jz)+\dots \tag{4}$$

In order to construct uniformly valid solutions for all distances downstream, all of the independent variables are perturbed following Crocco[8] and Lin,[9]

$$x=x_0+\epsilon x_1(x_0,y_0,jz_0)+\epsilon^2 x_2(x_0,y_0,jz_0)+\dots$$

$$y=y_0+\epsilon y_1(x_0,y_0,jz_0)+\epsilon^2 y_2(x_0,y_0,jz_0)+\dots$$

$$z=jz_0+j\epsilon z_1(x_0,y_0,jz_0)+j\epsilon^2 z_2(x_0,y_0,jz_0)+\dots \tag{5}$$

The relationship between the physical variables x, y, and z are the perturbation variables x_0, y_0, and z_0 evolves as part of the solution from the condition that the dependent variables remain uniformly valid functions of the independent variables in the far field. The shock shape in the form of an ordered expansion in ϵ is determined as part of the solution:

$$y_s(x,jz)=y_{s1}(x,jz)+\epsilon y_{s2}(x,jz)+\epsilon^2 y_{s3}(x,jz)+\dots \tag{6}$$

Substituting Eqs. (4) into Eqs. (1) and (2) and using Eq. (3) results, to $\mathcal{O}(\epsilon)$, in

$$\frac{\partial \rho_1}{\partial x}+\frac{\partial u_1}{\partial x}+\frac{\partial v_1}{\partial y}+j\frac{\partial w_1}{\partial z}=0 \tag{7a}$$

$$\frac{\partial \rho_1}{\partial x}+M_e^2\frac{\partial u_1}{\partial x}=0 \tag{7b}$$

$$\frac{\partial \rho_1}{\partial y}+M_e^2\frac{\partial u_1}{\partial x}=0 \tag{7c}$$

$$\frac{\partial \rho_1}{\partial z}+jM_e^2\frac{\partial w_1}{\partial x}=0 \tag{7d}$$

and to $\mathcal{O}(\epsilon^2)$ in

$$\frac{\partial \rho_2}{\partial x}+\frac{\partial u_2}{\partial x}+\frac{\partial v_2}{\partial y}+j\frac{\partial w_2}{\partial z}=-\frac{\partial(\rho_1 u_1)}{\partial x}-\frac{\partial(\rho_1 v_1)}{\partial y}-j\frac{\partial(\rho_1 w_1)}{\partial z} \tag{8a}$$

$$\frac{\partial \rho_2}{\partial x}+M_e^2\frac{\partial u_2}{\partial x}=-(\gamma-2)\rho_1\frac{\partial \rho_1}{\partial x}-M_e^2 u_1\frac{\partial u_1}{\partial x}-M_e^2 v_1\frac{\partial u_1}{\partial y}-jM_e^2 w_1\frac{\partial u_1}{\partial z} \tag{8b}$$

$$\frac{\partial \rho_2}{\partial y}+M_e^2\frac{\partial v_2}{\partial x}=-(\gamma-2)\rho_1\frac{\partial \rho_1}{\partial y}-M_e^2 u_1\frac{\partial v_1}{\partial x}-M_e^2 v_1\frac{\partial v_1}{\partial y}-jM_e^2 w_1\frac{\partial v_1}{\partial z} \tag{8c}$$

$$\frac{\partial \rho_2}{\partial z}+jM_e^2\frac{\partial w_2}{\partial x}=-j\left[(\gamma-2)\rho_1\frac{\partial \rho_1}{\partial z}+M_e^2\left(u_1\frac{\partial w_1}{\partial x}+v_1\frac{\partial w_1}{\partial y}+w_1\frac{\partial w_1}{\partial z}\right)\right] \tag{8d}$$

It is well known that entropy production is third order in shock strength, and it can be shown that it is nonzero only for terms of $\mathcal{O}(\epsilon^3)$ or higher.[10] Thus, starting with an isentropic source expansion, the shock-embedded flowfield is every-

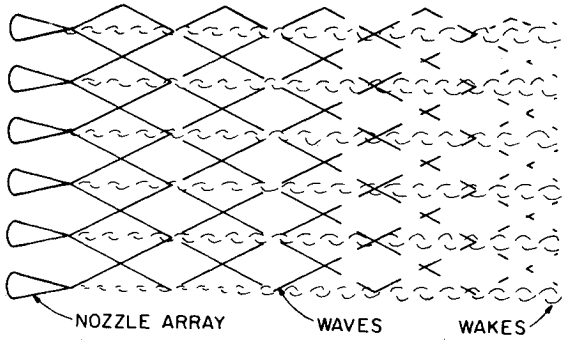

Fig. 1 Nonuniformities generated by 2-D nozzle array.

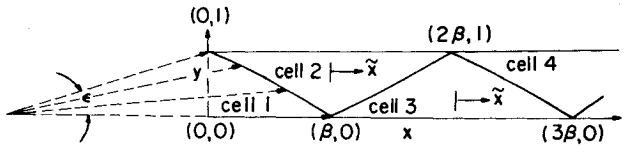

Fig. 2 Schematic of general problem.

where isentropic to $\mathcal{O}(\epsilon^2)$, while shock curvature is $\mathcal{O}(\epsilon)$. From the Crocco theorem, uniform entropy and total enthalpy require zero vorticity, i.e., the flow must still be irrotational. The fact that s_1 and s_2 are zero has been used in the above equations. While entropy changes do persist in the real flow, the accuracy of the solution to $\mathcal{O}(\epsilon^2)$ is not compromised by s changes introduced by a weak shock system.

Equations (7) and (8) are to be solved in each region or cell between successive shocks. The solution to $\mathcal{O}(\epsilon)$ and $\mathcal{O}(\epsilon^2)$ are found by applying the boundary conditions that the normal velocity is zero in all planes of symmetry, and that the product of the upstream and downstream normal velocity components across a shock is given by the appropriate form of Prandtl's relation,[3] while the tangential component remains unchanged. A uniformly valid solution is obtained for the nth cell if the relative magnitude of the terms of the expansion remains the same for all cell locations downstream. To develop such a solution, the appropriate expansion of the independent variables must be found which preserves the uniformity. In general, there is no guarantee that appropriate expansions can be found even for hyperbolic equations.

III. Plane Nozzle Array

Solution for the First Cell

The isentropic source flow in the first cell (see Fig. 2) is radial with streamlines given by

$$v/u = y(x+\cot\epsilon)^{-1} \tag{9}$$

Substituting Eqs. (4) and expanding for small ϵ yields

to $\mathcal{O}(\epsilon)$: $\quad v_1 = y$

and $\mathcal{O}(\epsilon^2)$: $\quad v_2 = u_1 y - v_1 x$

Eliminating ρ_1 from Eqs. (7b) and (7c) by cross differentiation and integrating the results gives

$$\frac{\partial u_1}{\partial y} = \frac{\partial v_1}{\partial x} + f(y)$$

where $f(y)=0$ as the flow is irrotational. Similarly, subtracting Eq. (7b) from Eq. (7a) and integrating results after substitution for v_1 in

$$u_1 = \beta^{-2}x + g(y)$$

where $\beta \equiv \sqrt{M_e^2-1}$. From the previous equations $g(y)$ can at most be constant; it is found to be zero as u_1 must be zero at (0,0). Thus,

$$u_1 = \beta^{-2}x, \quad v_1 = y, \quad \rho_1 = -M_e^2 u_1 \tag{10}$$

where ρ_1 was obtained from Eqs. (7b) and (7c) and the boundary condition at (0,0).

The solution to $\mathcal{O}(\epsilon^2)$ is obtained by first substituting Eq. (10) into the above $\mathcal{O}(\epsilon^2)$ expression for v_2, resulting in

$$v_2 = (2-M_e^2)\beta^{-2}xy$$

Again applying the condition of irrotationality,

$$\frac{\partial u_2}{\partial y} = (2-M_e^2)\beta^{-2}y$$

Now substituting Eqs. (10) and $\partial v_2/\partial y$ into Eqs. (8a) and (8b) and subtracting gives

$$\frac{\partial u_2}{\partial x} = -(\gamma M_e^4 - M_e^2 + 2)\beta^{-6}x$$

Thus u_2 may be integrated with the constant of integration evaluated by the condition that $u_2 = 0$ at (0,0). There results

$$u_2 = -D_1 M_e^{-2}\beta^{-2}x^2/2 - (M_e^2-2)\beta^{-2}y^2/2$$

$$v_2 = (2-M_e^2)\beta^{-2}xy \tag{11}$$

where

$$D_1 = M_e^2(\gamma M_e^2 - M_e^2 + 2)\beta^{-4}$$

These equations may be used with Eqs. (10) and (4) to predict the source flow in the first cell consistently to second order. ρ_2 may then be obtained by integrating Eqs. (8b) and (8c) and evaluating the constants.

Solution for the Second Cell

The second cell begins with the first shock origin at (0,1) in Fig. 2. For vanishingly small ϵ the shock coincides with the local Mach wave. Therefore, the shock shape can be expressed as a perturbation about a Mach wave

$$y_s = 1 - \beta^{-1}x + \epsilon S_1(x) + \epsilon^2 S_2(x)\ldots \tag{12}$$

where $S_1(x)$ and $S_2(x)$ are to be determined as part of the solution. Boundary conditions across y_s are that the tangential velocity remain unchanged and the normal component change in accordance with the conservation relations. The former leads to

$$(u\cos\alpha - v\sin\alpha)_u = (u\cos\alpha - v\sin\alpha)_d \tag{13}$$

where α is the local angle the shock makes with the x axis, and subscript u and d refer to conditions immediately upstream and downstream of y_s. Now,

$$\frac{dy_s}{dx} = -\tan\alpha = -\beta^{-1} + \epsilon\frac{dS_1}{dx} + \epsilon^2\frac{dS_2}{dx} \tag{14}$$

Substituting for $\tan\alpha$ in Eq. (13) and using Eqs. (4) yields to $\mathcal{O}(\epsilon)$

$$(u_1 - \beta^{-1}v_1)_d = (u_1 - \beta^{-1}v_1)_u$$

on y_s given by Eq. (12). From this and the linear dependence of u_{1u} and v_{1u} on x and y [Eqs. (10)] it is expected and can be shown that u_{1d} and v_{1d} are also linear.

The normal velocity is zero for all x at $y=1$. Thus, the most general solution for v_1 in the second cell which is linear in x and y is $v_1 = k_1(y-1)$. Again subtracting Eq. (7b) from Eq. (7a) and integrating results in $u_1 = \beta^{-2}k_1 x + k_2$. The $\mathcal{O}(\epsilon)$ boundary condition just developed from Eqs. (13) and (14) allows evaluation of the constants k_1 and k_2 giving the solution to $\mathcal{O}(\epsilon)$ as

$$u_1 = \beta^{-2}(x-\beta), \quad v_1 = y-1, \quad \rho_1 = -M_e^2 u_1 \tag{15}$$

where ρ_1 was obtained from Eqs. (7b) and (7c) with the constant of integration evaluated at (0,1) by application of the oblique shock relations for turning angle ϵ.

The Prandtl relation across an oblique shock can be written as[3]

$$(u\sin\alpha + v\cos\alpha)_u (u\sin\alpha + v\cos\alpha)_d = (\gamma+1)^{-1}[(\gamma-1) + 2M_e^{-2}] - (\gamma-1)(\gamma+1)^{-1}[u\cos\alpha - v\sin\alpha]_u^2 \tag{16}$$

where the left-hand side is the product of the upstream and downstream normal velocities. The first grouping on the right is the critical speed of sound squared, a constant evaluated at the origin, and the quantity in the second square bracket is the

tangential velocity component. Utilizing the expansions of Eqs. (14) and (4), there is obtained to $\mathcal{O}(\epsilon)$:

$$4(\gamma-1)^{-1}M_0^{-2}\beta\frac{dS_1}{dx}=\beta^{-2}(u_{1n}+u_{1d})+\beta^{-1}(v_{1u}+v_{1d})$$

$$+2(\gamma-1)(\gamma+1)^{-1}(u_{1u}-\beta^{-1}v_{1u})$$

which after integration and substitution of Eqs. (10) and (15), becomes

$$4S_1(x)=D_2\beta^{-1}x(x-\beta)$$

where (17)

$$D_2=M_e^2(\gamma M_e^2-3M_e^2+4)\beta^{-4}$$

Thus, this perturbation to the shock shape is a quadratic in x which vanishes at the ends, $x=0$ and β. Note that the shock intersects the nozzle axis at $x=\beta$ to $\mathcal{O}(\epsilon)$ as indicated in Fig. 2.

The solution to $\mathcal{O}(\epsilon^2)$ in the second cell may now be constructed. Following the procedure used for v_2 in the first cell, Eqs. (8) and (15) yield a wave equation which again has the solution form of Eqs. (11). Using Eq. (13) to replace $\tan\alpha$ in Eq. (14), and applying Eqs. (10) and (15) results in the second-order relation

$$(u_2-\beta^{-1}v_2)_d=\frac{dS_1}{dx}+(u_2-\beta^{-1}v_2)_u$$

on $y_s(x)$. From Eqs. (12) and (17), using the same logic as before, it is inferred that u_{2d} and v_{2d} are at most quadratic functions of x and y. The boundary condition that $v_2=0$ at $y-1$ then yields the most general form

$$v_2=C_1x(y-1)+C_2(y-1) \tag{18a}$$

where C_1 and C_2 are again unknown constants. From the condition of irrotationality,

$$\frac{\partial u_2}{\partial y}=C_1(y-1)$$

Using Eqs. (15) to evaluate the right-hand side of Eqs. (8a) and (8b), and substituting $\partial v_2/\partial y$ and then subtracting, there is obtained

$$\frac{\partial u_2}{\partial x}=-M_e^2(\gamma M_e^2-M_e^2+2)\beta^{-6}(x-\beta)+\beta^{-2}(C_1x+C_2)$$

Solving the last two equations

$$u_2=D_1\beta^{-2}(x^2/2-\beta x)+C_1\beta^{-2}x^2/2+C_2x$$

$$+C_1(y^2/2-y)+C_3 \tag{18b}$$

Substitution of Eqs. (18a) and (18b) into the second-order tangential velocity relation across the shock using Eq. (12) and the derivative of Eq. (17), and comparing coefficients

$$C_1=(2-M_e^2)\beta^{-2}$$

$$C_2=-(D_1/2+C_1)\beta+D_2\beta/4$$

$$C_3=C_1-D_2/4 \tag{18c}$$

Solution for the *n*th Cell

The procedure used to solve for the flow variables in the second cell may be repeated sequentially for later cells. With the origin shifted such that $\tilde{x}$ is measured from the center of each cell, the solution becomes $\mathcal{O}(\epsilon)$:

$$u_1=\beta^{-2}\tilde{x},\quad v_1=y-\delta,\quad \rho_1=-M_e^2u_1 \tag{19}$$

here $\tilde{x}=x-(n-1)\beta$ and $\delta=0$ for n odd and unity for n even. To $\mathcal{O}(\epsilon^2)$,

$$u_2=(C_1-D_1)\beta^{-2}\tilde{x}^2/2+C_4\beta^{-2}\tilde{x}+C_1(y^2/2-\delta y)+C_5$$

$$v_2=(C_1+C_4\tilde{x}/2)(y-\delta) \tag{20a}$$

where C_1, C_2, C_3, D_1, and D_2 are given by Eqs. (11), (17), and (18c), and

$$C_4=C_1\beta-(n-1)(D_1\beta/2-D_2\beta/4)$$

$$C_5=C_3+(n-2)D_2/4 \tag{20b}$$

It may be easily verified that Eqs. (20a) and (20b) reproduce Eqs. (10) and (11) and Eqs. (15) and (18) for the first and second cells, respectively. While the $\mathcal{O}(\epsilon)$ solutions of Eqs. (20) are undecaying, the magnitude of the $\mathcal{O}(\epsilon^2)$ perturbations increases with n, presenting a classic example of loss of solution validity for large values of independent variable. The standard correction procedure is to employ the idea of coodinate perturbation or matched asymptotic expansion involving multiple scales.[11] Following Crocco,[8] each term on the right-hand side of Eqs. (4) is expanded in a separate Taylor series about the point $\tilde{x}_0,y_0$. Substituting Eqs. (5) for $\tilde{x}$-$\tilde{x}_0$ and y-y_0,

$$u_1(\tilde{x},y)=u_1(\tilde{x}_0,y_0)+(\epsilon x_1+\epsilon^2x_2+\ldots)\frac{\partial u_1(\tilde{x}_0,y_0)}{\partial\tilde{x}_0}$$

$$+(\epsilon y_1+\epsilon^2y_2+\ldots)\frac{\partial u_1(\tilde{x}_0,y_0)}{\partial y_0}$$

where x_1,y_1, etc., are functions of $\tilde{x}_0$ and y_0. Further, the equation is exact as u_1 has been shown to be at most linear in $\tilde{x}_0$ and y_0; similar expressions for $u_2(\tilde{x},y)$ may have second-derivative terms. Substituting these and similar expressions into Eqs. (4) there is obtained to $\mathcal{O}(\epsilon)$

$$u(\tilde{x},y)=1+\epsilon u_1(\tilde{x}_0,y_0)+\epsilon^2\left[u_2(\tilde{x}_0,y_0)\right.$$

$$\left.+x_1\frac{\partial u_1}{\partial\tilde{x}_0}(\tilde{x}_0,y_0)+y_1\frac{\partial u_1}{\partial y_0}(\tilde{x}_0,y_0)\right]+\ldots$$

$$v(\tilde{x},y)=v_0(\tilde{x},y_0)+\epsilon v_1(\tilde{x}_0,y_0)+\epsilon^2\left[v_2(\tilde{x}_0,y_0)\right.$$

$$\left.+x_1\frac{\partial v_1}{\partial\tilde{x}_0}(\tilde{x}_0,y_0)+y_1\frac{\partial v_1}{\partial y_0}(\tilde{x}_0,y_0)\right]+\ldots \tag{21}$$

where the u_1,u_2, etc., refer to the solutions already obtained without coordinate stretching, that is, with $\tilde{x}=\tilde{x}_0$, $y=y_0$, and no ϵ dependence for $\tilde{x}$ and y. From Eqs. (5) the relationship between the physical coordinates $\tilde{x}$ and y and the strained coordinates $\tilde{x}_0,y_0$ gets progressively modified as the solution is carried to higher order. The x_1,y_1, etc., functions that occur are to be determined to cancel the terms causing the loss of validity at each higher order.

Equating the ϵ^2 terms in Eqs. (4) and (21) and applying Eqs. (19),

$$u_2(\tilde{x},y)=u_2(\tilde{x}_0,y_0)+\beta^{-2}x_1$$

$$v_2(\tilde{x},y)=v_2(\tilde{x}_0,y_0)+y_1$$

Choosing x_1 and y_1 to cancel the terms which build up with n,

$$x_1 = \alpha_1 \tilde{x}_0 - (C_5 - C_3)\beta^{-2} \text{ and } y_1 = \alpha_1 (y_0 - \delta) \tag{22a}$$

where

$$\alpha_1 = -D_1\beta/2 + D_2\beta/4 \tag{22b}$$

The solutions for u_1 and v_1 remain unchanged and are given by Eqs. (19) with $\tilde{x} = \tilde{x}_0$, $y = y_0$; however, to $\mathcal{O}(\epsilon^2)$

$$u_2 = (C_1 - D_1)\beta^{-2}\tilde{x}_0^2/2 - C_1\beta^{-1}\tilde{x}_0 + C_1(y_0^2/2 - \delta y_0) + C_3$$

$$v_2 = C_1\tilde{x}_0(y_0 - \delta)$$

where the n dependence from C_4 and C_5 has now disappeared. Applying Eqs. (22) to Eqs. (5) to $\mathcal{O}(\epsilon)$ and rearranging

$$\tilde{x}_0 = \frac{\tilde{x}}{1+\epsilon\alpha_1} + \frac{\epsilon(C_5 - C_3)\beta^{-2}}{1+\epsilon\alpha_1}, \quad y_0 - \delta = \frac{y - \delta}{1+\epsilon\alpha_1}$$

Inserting these expressions into the u_1, v_1, u_2, and v_2 solutions above, Eqs. (4) can be written to $\mathcal{O}(\epsilon^2)$

$$u = 1 + \frac{\epsilon}{1+\epsilon\alpha_1}\beta^{-2}\tilde{x} + \frac{\epsilon^2}{(1+\epsilon\alpha_1)^2}\left[(C_1 - D_1)\beta^{-2}\frac{\tilde{x}^2}{2}\right.$$

$$\left. - C_1\beta^{-1}\tilde{x} + C_1\left(\frac{y^2}{2} - \delta y\right) + C_3\right] + \frac{\epsilon^2}{(1+\epsilon\alpha_1)^2}(C_5 - C_3)\beta^{-2}$$

$$v = \frac{\epsilon}{1+\epsilon\alpha_1}(y - \delta) + \frac{\epsilon^2}{(1+\epsilon\alpha_1)^2}C_1(y - \delta)\tilde{x} \tag{23}$$

Comparing Eqs. (23) for $n = 2$ with Eqs. (10) and (11) for the first cell were $x = \tilde{x}$, it can be seen that the flow in the second cell is radial with angle $\epsilon(1+\epsilon\alpha_1)^{-1}$ and the origin transferred to $y = 1$. The effect of the first shock is to cause the angle to decay from ϵ to $\epsilon(1+\epsilon\alpha_1)^{-1}$, to shift the y origin, and to introduce a change in the reference value of u to $\mathcal{O}(\epsilon^2)$. The solution in the third cell is similarly related to that in the second. Thus, the angle for the third cell is $\epsilon(1+2\epsilon\alpha_1)^{-2}$ to $\mathcal{O}(\epsilon^2)$ and the change in reference value becomes

$$\epsilon^2\left[\frac{1}{1+\epsilon\alpha_1} + \frac{1}{(1+\epsilon\alpha_1)(1+2\epsilon\alpha_1)}\right](C_5 - C_3)\beta^{-2}$$

Generalizing and substituting for the constants, the $\mathcal{O}(\epsilon)$ solution in the nth cell replacing Eqs. (19) can be written from Eqs. (23) as

$$u_1 = \beta^{-2}\tilde{x}(1 + (n-1)\alpha_1\epsilon)^{-1}, \quad v_1 = (y - \delta)(1 + (n-1)\alpha_1\epsilon)^{-1}$$

$$\rho_1 = -M_e^2 u_1 \tag{24}$$

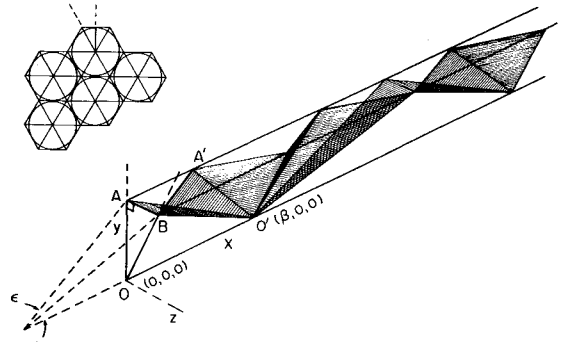

Fig. 3 Source flow into basic 30 deg right-triangular channel (insert shows close-packed exit geometry leading to hexagonal confinement).

with $\alpha_1 = (\gamma+1)M_e^4\beta^{-3}/4$ from Eq. (22b).

The $\mathcal{O}(\epsilon^2)$ uniformly valid solution is also available[12]; both are applicable as long as $\beta\tan\epsilon < 1$.

IV. Three-Dimensional Flow

Basic Geometry

A closely packed nozzle array is considered, with resultant minimum internozzle area, as shown on the insert of Fig. 3. Each nozzle flow is axially symmetric prior to leaving the array, and being identical with its neighbors must share equal space downstream. Thus, it is expected that each downstream flow will behave as if constrained by a solid boundary of hexagonal cross section that circumscribes the circular nozzle exit. This unusual geometry provides relief from the fact that an axisymmetric flow could not remain fully supersonic, as a convergent axisymmetric shock reflects as a Mach shock off the axis regardless of initial strength.[9] By symmetry, the present flow is built up of channels with 30 deg right-triangular cross section. As seen on the figure, these have vertices at the center and one corner of a hexagon, together with the midpoint of the side containing the corner. The flow from each nozzle is formed from 12 such channels.

Figure 3 shows 3-D source flow into a 30-deg right-triangular channel and the associated shock system. The source flow is taken to be hexagonal in cross section rather than conical, an assumption consistent with the order of the solution sought. In addition to the main shock of the plane flow case, shock reflections from its contact with the plane OB are now required to turn the flow parallel at that boundary. These shocks successively reflect between planes OA and OB, combining with the main shock to form the system shown on Figs. 3 and 4. While not obvious, the existence of a repetitive shock pattern will be formally shown by consideration of the flow to $\mathcal{O}(\epsilon)$; the actual decay will again necessitate solution to $\mathcal{O}(\epsilon^2)$.

Cartesian coordinates are again chosen, with x along the nozzle axis and y and z parallel to the orthogonal sides of the triangular element. The solution proceeds from Eqs. (5-8) with $j = 1$ and the boundary condition that the normal velocity must vanish on each of three planes formed by the side of the right triangle and the nozzle axis.

Repetitive Solution

To start the calculation, the flow upstream of the first shock can be solved as in Sec. III to give to $\mathcal{O}(\epsilon)$

$$u_1 = 2\beta^{-2}x, \quad v_1 = y, \quad w_1 = z \quad \text{and} \quad \rho_1 = -M_e^2 u_1 \tag{25}$$

and to $\mathcal{O}(\epsilon^2)$

$$u_2 = (M_e^4 - 2\gamma M_e^4 - 3)\beta^{-6}x^2 + (M_e^2 - 3/2\beta^2)\beta^{-2}(y^2 + z^2)$$

$$v_2 = (3 - M_e^2)\beta^{-2}xy$$

$$w_2 = (3 - M_e^2)\beta^{-2}xz \tag{26}$$

This source flow is divergent, having velocity component $v_1 = 1$ to $\mathcal{O}(\epsilon)$ along AB. The boundary condition on the top

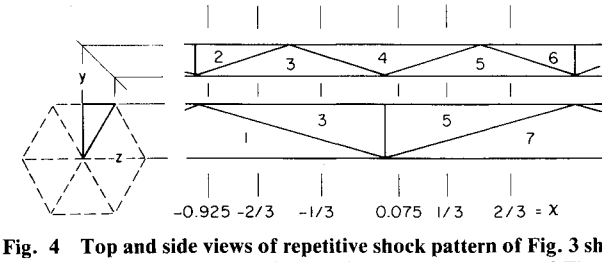

Fig. 4 Top and side views of repetitive shock pattern of Fig. 3 showing location of numbered regions and constants χ planes of Fig. 5.

plane leads to an oblique shock propagating inward. Again, following the procedure of Sec. II, the flow properties immediately downstream are, to $\mathcal{O}(\epsilon)$

$$u_1=\beta^{-2}(2x-\beta),\quad v_1=y-1,\quad w_1=z,\quad \text{and}\quad \rho_1=-M_e^2u_1 \tag{27}$$

Note that w_1 is unchanged from Eqs. (25), and that u_1 is twice the value given in Eqs. (15).

While Eqs. (27) satisfy the top and vertical plane boundary conditions, they produce a normal velocity on the inclined plane given by $v_1\sin 30-w_1\cos 30=-\epsilon/2$ at $z=y/\sqrt{3}$. For small ϵ, the disturbance due to a change in boundary conditions at a point will propagate within a Mach cone extending downstream. Thus, the change initiated along BO′ in Fig. 3 is contained within a family of Mach cones. Let a point on BO′ be characterized by ξ such that

$$\beta^{-1}x=1-\xi,\qquad z=\xi\tan 30$$

The equation for the intersection of the Mach cone from ξ with the $z=0$ plane is then

$$(y-\xi)^2+\xi^2\tan^2 30=(\beta^{-1}x-1+\xi)^2$$

The shock shape is the envelope of these parabolas and is seen to be planar by eliminating ξ between this equation and its ξ derivative. It is given by[12]

$$\beta^{-1}x=1-y(2\cos^2 30-1)=1-y/2,\qquad z=0 \tag{28}$$

To $\mathcal{O}(\epsilon)$, A′BO′ is thus a plane representing the upstream extent of the disturbance. The boundary conditions are satisfied if this is an oblique shock sheet with velocity components behind it given through now familiar analysis[12] as

$$u_1=\beta^{-2}(2x-3/2\beta),\quad v_1=y-1,\quad w_1=z-1/\sqrt{3},$$
$$\text{and}\quad \rho_1=-M_e^2u_1 \tag{29}$$

This shock similarly reflects as a shock from the vertical plane with downstream flow to $\mathcal{O}(\epsilon)$

$$u_1=\beta^{-2}(2x-2\beta),\quad v_1=y-1,\quad w_1=z,\quad \text{and}\ \rho_1=-M_e^2u_1 \tag{30}$$

At $x=\beta$ half of the reflection cycle is complete. The main shock has reached the nozzle axis and the two side shocks have alternated the sign of w_1 while reducing u_1. The flow is source-like with negative v_1. Further downstream the main shock reflects upward and the side shock undergoes two additional reflections as seen on Figs. 3 and 4. The flow is turned by these shocks, to finally re-emerge identical to the original radial source flow to $\mathcal{O}(\epsilon)$. The complete flow must then repeat to this order.

It is useful to define $\chi=\beta^{-1}x-(n-1)$ for even n cells. Then $\chi=0$ where the main shock meets the axis and $-1\le\chi\le 1$ encompasses the repetitive flow pattern as shown in Fig. 4. Its solution may then be re-expressed from Eqs. (25) and (27-30) as

$$u_1=\beta^{-1}F(\chi),\quad v_1=G(y),\quad w=H(z),\quad \text{and}\quad \rho_1=-M_e^2u_1 \tag{31}$$

where $F(\chi)$ for the various regions is indicated on Fig. 5. This figure shows slices through Figs. 3 and 4 at constant χ. The lines within the triangles are the shocks which separate the flow regions. As χ increases, the main shock between regions 1 and 2 advances toward the nozzle axis, and the side shock that satisfies the inclined-plane boundary condition moves out

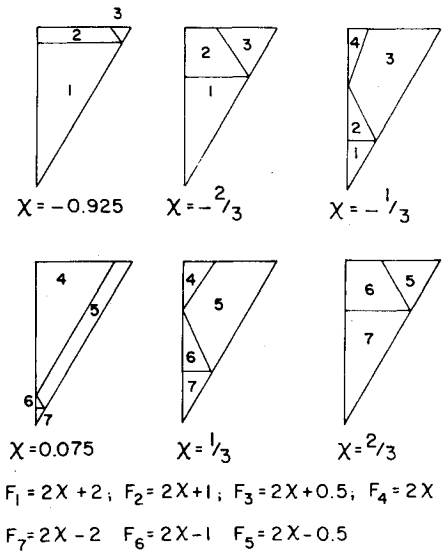

Fig. 5 Shock geometry in constant χ planes and values of $F(\chi)$.

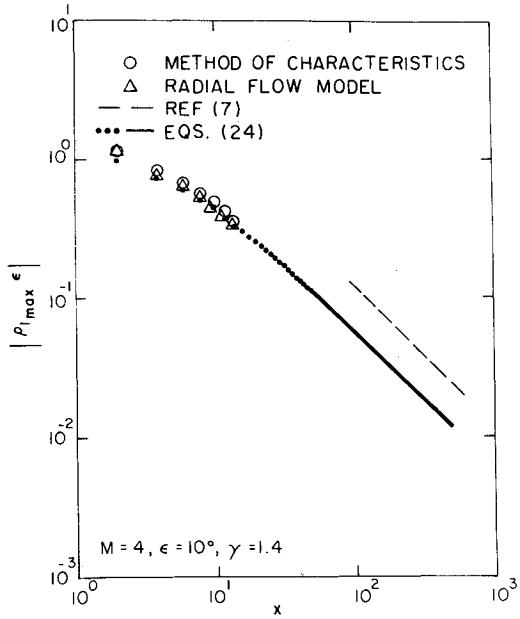

Fig. 6 Decay of $\rho_{1_{max}}\epsilon$ in 2-D flow.

from the corner to subsequently reflect off the line of vertical symmetry. $G(y)=y$ in regions 1 and 7 and $y-1$ elsewhere, while $H(z)=Z-1/\sqrt{3}$ in regions 3 and 5 and z elsewhere. The perturbed pattern repeats itself every time the main shock reflects back to the outer boundary, i.e., every 2χ.

Flow Decay

The equation describing the $\mathcal{O}(\epsilon)$ correction to the main shock shape is obtained by the procedure used for Eq. (17) as

$$2S_1(x)=M_e^2\beta^{-3}x^2+D_2\beta^{-1}x(x-\beta/2) \tag{32}$$

Note that this shock meets the nozzle axis farther downstream than $x=\beta$ due to the fact that u_1 is changing twice as rapidly as in the planar case.

Eliminating the ρ derivative between Eqs. (8a) and (8b) and substituting Eqs. (27) for the flow behind the shock,

$$\frac{\partial u_2}{\partial x}=(3-M_e^2)\beta^{-2}x+4D_1x+\frac{\partial v_2}{\partial y}$$

Similarly, cross differentiation of Eqs. (8b) and (8c) and substitution of this result with Eqs. (27) yields the wave equation for v_2 with solution form

$$v_2 = f_1(x+\beta y) + f_2(x-\beta y)$$

With conditions that v_2 is zero on the $y=1$ plane and the tangential velocity is unchanged across the shock the solution can be shown as[12]

$$v_2 = [(3-M_3^2)\beta^{-2}x + C_6](y-1)$$

$$u_2 = 2D_1\beta^{-2}(x^2 - x\beta) + (3-M_e^2)\beta^{-4}x^2 + C_6\beta^{-2}x + (3-M_e^2)\beta^{-2}(y-1)^2/2 + D_3/2 \quad (33)$$

where

$$C_6 = -D_1\beta - (3-M_e^2)\beta^{-1} + D_3\beta^2/2$$

$$D_3 = M_e^2(\gamma M_e^2 - 2M_e^2 + 3)\beta^{-4}$$

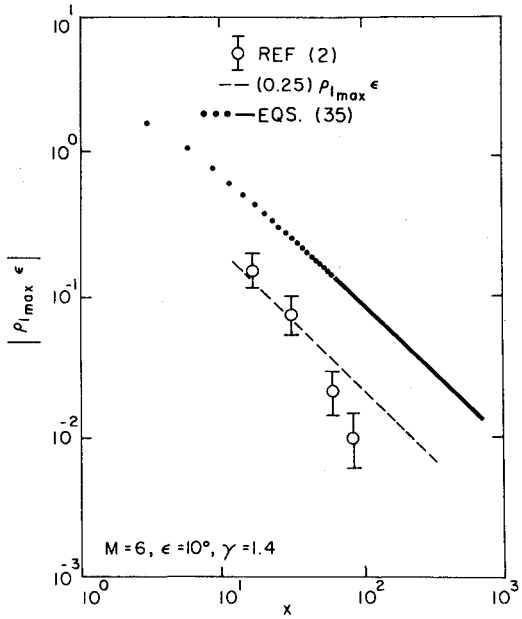

Fig. 7 Decay of $\rho_{1_{max}}\epsilon$ in 3-D flow.

Closely following Sec. III, Eqs. (27) and (33) are generalized for the nth cell, and then expressed in terms of strained coordinates to yield new $\mathcal{O}(\epsilon)$ relations:

$$u_1 = 2\beta^{-2}\bar{x}(1+(n-1)\alpha_2\epsilon)^{-1}$$

$$v_1 = (y-\delta)(1+(n-1)\alpha_3\epsilon)^{-1} \quad (34)$$

where

$$\alpha_2 = 3D_1\beta/2 - D_3\beta^2/4 - (3-M_e^2)\beta^{-1}/2$$

$$\alpha_3 = D_1\beta - D_3\beta^2/2$$

Unlike the plane case, two different angle coefficients are needed; however, all velocity components must ultimately decay at the same rate after passing through a complete shock cycle. Thus superimposing the decay of the main shock on the repetitive pattern of Eqs. (33) there is obtained:

$$u_1 = \beta^{-1}F(\chi)(1+(n-1)\alpha_2\epsilon)^{-1}$$

$$v_1 = G(y)(1+(n-1)\alpha_3\epsilon)^{-1}$$

$$w_1 = H(z)(1+(n-1)\alpha_3\epsilon)^{-1}, \text{ and } \rho_1 = -M_e^2 u_1 \quad (35)$$

for the close packed 3-D solution equivalent to Eqs. (24).

V. Discussion and Application

Density uniformity is often important for flows involving radiation, such as laser cavities, and may be measured directly with interferometry. Thus, it is convenient to choose the ρ_1 predictions of Eqs. (24) and (35) for comparison with other theory, numerical calculation, and available experimental results.

Ignoring the decay term and evaluating $\bar{x}$ in adjacent cells, Eqs. (24) predict a jump in ρ_1 across each cell-bounding shock of $M_e^2\beta^{-1}$, the flow being subsequently reaccelerated to be shocked again. The maximum ρ_1 value within a cell ($\rho_{1_{max}}$) is also equal to $M_e^2\beta^{-1}$. This decays downstream with increasing n due to the $(1+(n-1)\alpha_1\epsilon)^{-1}$ factor. The x location for each cell center ($\bar{x}=0$) is given by $(n-1)\beta$, and $|\rho_{1_{max}}\epsilon|$ is plotted vs this position on Fig. 6 for the specific case of a 2-D nozzle of $\epsilon = 10$ deg expanded to $M_e = 4$ in a $\gamma = 1.4$ gas. While a dot is shown at each cell center, these merge together at large x due to the logarithmic abscissa.

The maximum local perturbation for large n becomes

$$|\rho_{1_{max}}\epsilon| \approx M_e^2(n\alpha_1\beta)^{-1} = 4(M_e^2-1)^{3/2}[(\gamma+1)M_e^2 x]^{-1} \quad (36)$$

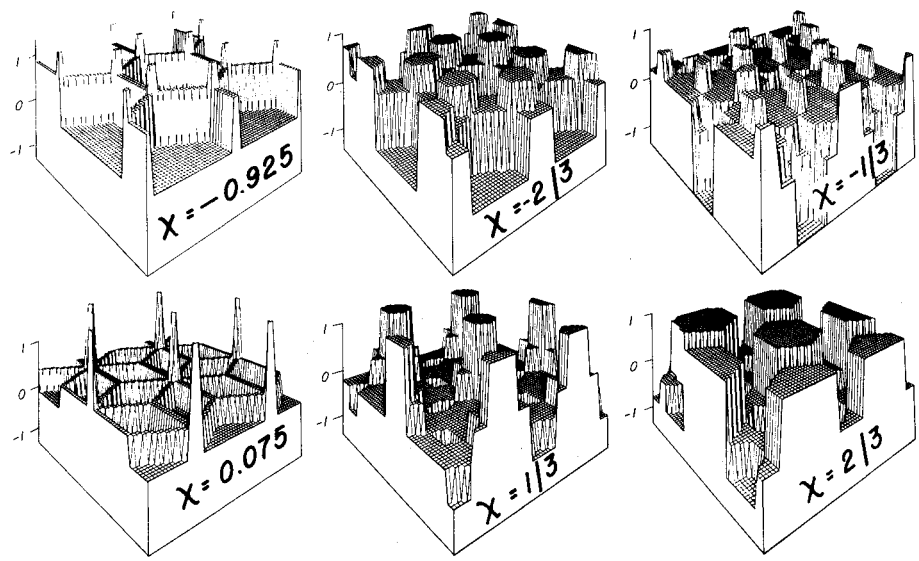

Fig. 8 Cross-sectional distribution of ρ perturbation at fixed χ (vertical axis in units of $\rho_1 M_e^{-2}\beta$).

This decays inversely with x such that the maximum value in a cell falls to the percent level at 500 nozzle half-heights downstream. Simons' result[7] is also shown; with the factor of 2 difference attributable to the location of the origin in the present case through uniformly valid analysis. The near-field decay rate appears slower on the figure, but is much faster on a linear plot. The disturbance level here is slightly lower than method-of-characteristics calculations that include s variation, however, it should be noted that $\beta\tan\epsilon$ is close to 1 for this example [see statement after Eq. (24)]. Near-field agreement is also seen with a model that uses shocks with s variation, but assumes that the flow behind each wave remains radial.[12]

The 3-D close-packed solution is more complex. Equations (31) and Fig. 5 show that the ρ_I jump across the main shock has the same value as in the 2-D case, with one-half that value across the side shocks. On the other hand, Fig. 5 predicts a maximum local disturbance amplitude of 2, and so

$$|\rho_{I_{\max}}\epsilon| \approx 2M_e^2(n\alpha_2\beta)^{-1} = 8(\gamma+1)M_e^2(M_e^2-1)^{3/2} \times [4(\gamma+1)M_e^2+\gamma M_e^2-6M_e^2+1+6M_e^{-2}]\,[(\gamma+1)M_e^2x]^{-1} \tag{37}$$

This is again inverse with x, with value close to Eq. (36) for the same conditions, and the $M_e=6$ case of Fig. 7 now requiring 10^3 nozzle half-heights to drop to the percent level. While the ratio of the 3-D to 2-D decay rate is M_e dependent, it approaches one at high M_e. The data shown on Fig. 7 were obtained by reading the maximum local fringe excursion on interferograms taken with optical axis aligned vertically through the nozzle pattern sketched on Fig. 3 ($\phi=0$). The $\rho_{I_{\max}}$ from Eqs. (35) is seen to be well above the error bars for these measurements. This will be explained in the following discussion.

Figure 8 presents cross-sectional views of the ρ perturbation at the fixed χ values of Figs. 4 and 5. These were obtained from Eqs. (31) with $-2\le y,\ z\le 2$ plotted in the horizontal plane and units of $\rho_I M_e^{-2}\beta$ in the vertical. The hexagonal structure of the flow is clearly indicated by the main shock from the nozzle boundaries in the $\chi=-0.925$ view. This shock retains the unit rise in ordinate value as χ increases, but moves toward the nozzle axes into a ρ level reduced by the source-like expansion. The side shocks and their reflections rapidly become prominent features. ρ_I goes to zero at $\chi=0$, however $\rho_{I_{\max}}$ occurs immediately on either side of $\chi=0$ as suggested by the sharp peaks at $\chi=0.075$. The perturbation is antisymmetric about $\chi=0$, and thus the $\chi=1/3$ and $2/3$ views are inversions of the $\chi=-1/3$ and $-2/3$ views, respectively. An interferometer measures difference in ρ integrated along optical paths, and the structure of Fig. 8 makes it clear that the theoretical $\rho_{I_{\max}}$ line in Fig. 7 would be expected to overestimate the measurements substantially.

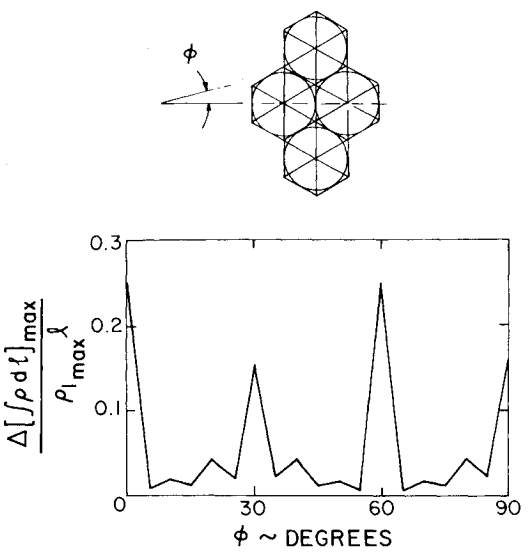

Fig. 9 Maximum difference in optical integral vs optical axis orientation.

Figure 9 results from numerically integrating ρ along optical paths of length ℓ normal to the flow. The transverse location was varied at fixed χ and the maximum difference in $\int\rho d\ell$ found vs χ. In turn, the maximum value of this difference was normalized by $\rho_{I_{\max}}\ell$ and plotted as the ordinate on the figure. The calculations were then repeated for different values of the angle ϕ that the optical path makes with the nozzle pattern, as defined in the figure. All calculations were carried out for an ℓ of 200 nozzle half-heights to provide adequate pattern integration at intermediate values of ϕ. It can be seen that the maximum optical path difference is 0.25 $\rho_{I_{\max}}\ell$ at $\phi=0$. This difference produces the fringes on the interferograms, and thus comparison with the data of Fig. 7 requires reduction of the $\rho_{I_{\max}}$ theoretical result by 0.25. The agreement is then satisfactory. Further, it can be seen from Fig. 9 that selection of ϕ can reduce the effective ρ perturbation by more than an additional order of magnitude due to the smearing out of the integrated differences, with prominent peaks remaining at symmetry angles that are multiples of 30 deg.

The effect of ϕ on laser beam quality can be important, and recent experimental studies have confirmed the substantial reduction of integrated disturbance with ϕ, and that the peak value of the ordinate on Fig. 9 occurs at $\chi=\pm 0.5$ with reversed sign.[13] The full solution of the disturbance field also has application to flows where rate processes are sensitively dependent on local conditions.

VI. Conclusions

Uniformly valid solutions have been developed for the decay of weak waves from 2-D and 3-D nozzle arrays. The 2-D solution exhibits the remarkable property that the wave system generated by a radial supersonic flow entering a constant height channel retains radial streamlines to $\mathcal{O}(\epsilon^2)$. This allows the solution to be simply expressed as a repetitive disturbance with a superimposed decay. The result is found to be in reasonable agreement with variable-entropy numerical and source-flow model predictions in the near field, with a factor of 2 difference over a previously reported far-field result.

The waves from a close-packed array of 3-D radial nozzles have been analyzed under the assumption of hexagonal symmetry. It is found that Mach reflection off the axis does not occur. Instead, there exists a repetitive shock pattern consisting of six planar shock sheets, again with a simple decay superimposed. The results of the analysis compare favorably with available experimental data once the 3-D nature of the field is properly accounted for. Many observed features are predicted by the model, including a substantial effect of optical angle on integrated disturbance level. Thus verified, the present modeling procedure can serve as the starting point for study of the flow perturbations from other nozzle array configurations.

Acknowledgment

The work contained herein was supported by the Air Force Office of Scientific Research under Grant 77-3450 and Contract F49620-79-C-0020.

References

[1]Royle, J. K., Bowling, A. G., and Lukasiewicz, J., "Calculation of Two-Dimensional and Conical Supersonic Multi-Nozzles," RAE AERO 2221, S.D. 23, 1947.

[2]Russell, D. A., Neice, S. E., and Rose, P. H., "Screen Nozzles for Gasdynamic Lasers," *AIAA Journal*, Vol. 13, May 1975, pp. 593-599.

[3]Courant, R. and Friedrich, K. O., *Supersonic Flow and Shock Waves*, 1st Ed., Springer-Verlag, New York, 1976, Chaps. IV and VI.

[4]Lighthill, M. J., "A Technique for Rendering Approximate Solution to Physical Problems Uniformly Valid," *Philosophical Magazine*, Vol. 40, July 1949, pp. 1179-1201.

[5]Whitham, G. B., "The Behavior of Supersonic Flow Past a Body of Revolution Far from the Axis," *Proceedings of the Royal Society of London*, Ser. A, Vol. 201, March 1950, pp. 89-108.

[6]Whitham, G. B., "The Flow Pattern of a Supersonic Projectile," *Communications on Pure and Applied Mathematics*, Vol. 5, Aug. 1952, pp. 301-349.

[7]Simons, G. A., "Decay of a Diamond Shock Pattern," *AIAA Journal*, Vol. 10, Aug. 1972, pp. 1037-1043.

[8]Crocco, L., "Coordinate Perturbation and Multiple Scales in Gasdynamics," *Philosophical Transactions of the Royal Society*, Ser. A, Vol. 272, June 1972, pp. 275-301.

[9]Lin, C. C., "On a Perturbation Theory Based on the Method of Characteristics," *Journal of Mathematics and Physics*, Vol. 33, July 1954, pp. 117-134.

[10]Liepmann, H. W. and Roshko, A., *Elements of Gasdynamics*, 1st ed., John Wiley & Sons, New York, 1957, p. 60.

[11]VanDyke, M., *Perturbation Methods in Fluid Mechanics*, 1st ed., Academic Press, New York, 1964, p. 78.

[12]Vaidyanathan, T. S., "Wave Decay Downstream of a Nozzle Array," Ph.D. Thesis, University of Washington, Seattle, Wash., 1979.

[13]Russell, D. A. and Chu, Y. K., "Aerodynamic Disturbances from Supersonic Nozzle Arrays," to be published in *Proceedings of 4th International Symposium on Gas Flow and Chemical Lasers*, edited by M. Onorato, Politecnico de Torino, Italy.